# Thermochemical Stabilities and Structures of the Cluster Ions $OCS^+$, $S_2^+$, $H^+(OCS)$, and $C_2H_5^+$ with OCS Molecules in the Gas Phase

K. Hiraoka, K. Fujita, M. Ishida, K. Hiizumi, F. Nakagawa, and A. Wada
Clean Energy Research Center, University of Yamanashi, Kofu, Japan

S. Yamabe and N. Tsuchida
Department of Chemistry, Nara University of Education, Nara, Japan

The gas-phase clustering reactions of $OCS^+$, $S_2^+$, $H^+(OCS)$, and $C_2H_5^+$ ions with carbonyl sulfide (OCS) molecules were studied using a pulsed electron-beam high-pressure mass spectrometer and applying density functional theory (DFT) calculations. In the cluster ions $OCS^+(OCS)_n$ and $H^+(OCS)(OCS)_n$, a moderately strong, here referred to as "semi-covalent", bond was formed with $n = 1$. However, the nature of bonding changed from semi-covalent to electrostatic with $n = 1 \rightarrow 2$. The bond energy of $S_2^+(OCS)$ was determined experimentally to be 12.9 ± 1 kcal/mol, which is significantly smaller than that of the isovalent $S_2^+(CS_2)$ complex (30.9 ± 1.5 kcal/mol). DFT based calculations predicted the presence of several isomeric structures for $H^+(OCS)(OCS)_n$ complexes. The bond energies in the $C_2H_5^+(OCS)_n$ clusters showed an irregular decrease for $n = 1 \rightarrow 2$ and $7 \rightarrow 8$. The nonclassical bridge structure for the free $C_2H_5^+$ isomerized to form a semi-covalent bond with one OCS ligand, $[H_3CCH_2 \cdots SCO]^+$, i.e., reverted to classical structure. However, the nonclassical bridge structure of $C_2H_5^+$ was preserved in the cluster ions $C_2H_5^+(OCS)_n$ below 140 K attributable to the lack of thermal energy for the isomerization. DFT calculations revealed that stability orders of the geometric isomers of $H^+(OCS)(OCS)_n$ and $C_2H_5^+(OCS)_n$ changed with increasing $n$ values. (J Am Soc Mass Spectrom 2005, 16, 1760–1771) © 2005 American Society for Mass Spectrometry

Carbonyl sulfide (OCS) plays an important role in the global cycling of sulfur [1]. The compound is released into the atmosphere by oceans, biomass burning, oxidation of $CS_2$, as well as by anthropogenic sources, e.g., tire wear, aluminum production, coal combustion, and sulfur recovery. Terrestrial vegetation, soils, and photolysis help to remove it from the atmosphere [2]. OCS is the major source of stratospheric background aerosol because of its high abundance (~500 ppt) and long lifetime (2–7 y) in the troposphere. Owing its physico-chemical properties, OCS contributes significantly to the earth's radiation budget and is of considerable importance in heterogeneous reactions involved in chemical ozone destruction [3]. The compound has also been detected in the interstellar medium [2].

Ionic complexes are key constituents of interstellar matter and are essential to many chemical processes on earth. Although studies of ion/molecule reactions are subject to extensive investigations, such studies for OCS are scarce.

Ono et al. [4] investigated molecular beam photoionization of $(OCS)_n$, $n$ = 1–3, and $OCS \cdot CS_2$. From the measured ionization energies of $(OCS)_n$, $n$ = 1 and 2, and $OCS \cdot CS_2$, the binding energies for $OCS^+(OCS)$ and $CS_2^+(OCS)$ were computed as 17.2 ± 1 and 5.6 ± 1 kcal/mol, respectively. McKee [5] performed an ab initio study on $OCS^+(OCS)$ and predicted that this species is bound by a *two-center three-electron* bond between the two sulfur atoms. At the UHF/6–31G* level, the lowest energy structure had $C_2$ symmetry with a S···S distance of 2.866 Å. At the [MP4/6-31 + G*]+ZPE level, the bond energy was calculated to be 19.9 kcal/mol. Jacox et al. studied infrared spectra of $OCS^+$ and $OCS^-$ trapped in solid neon [6]. With the codeposition of microwave-excited Ne:OCS at 5 K, the spectrum of the resulting deposit showed absorptions which they assigned to $OCS^+$, $OCS^-$, and one or more dimer ions.

In the present work, clustering reactions of four cationic species, $OCS^+$, $S_2^+$, $H^+(OCS)$, and $C_2H_5^+$, with

Published online September 26, 2005

Address reprint requests to Dr. K. Hiraoka, Clean Energy Research Center, University of Yamanashi, Takeda 4-3-11, Kofu 400-8511, Japan. E-mail: hiraoka@ab11.yamanashi.ac.jp


1044-0305/05/$30.00
doi:10.1016/j.jasms.2005.07.007

Received August 10, 2004
Revised July 22, 2005
Accepted July 22, 2005

OCS molecules have been investigated both experimentally and theoretically. The results indicate the existence of several isomeric structures for the cluster ions. The study demonstrates that while the interaction of the negatively charged O atom of OCS with a cation is mainly electrostatic in nature, the nearly neutral S atom of OCS forms a strong bond, here referred to as "semi-covalent", with the cation.

## Experimental and Computational Methods

The experiments were performed with a pulsed electron-beam high-pressure mass spectrometer (HPMS) [7, 8]. The equilibria for clustering reaction were established in the HPMS experiments immediately following the electron pulse, and equilibrium constant measurements were straightforward. The carrier gas, which was either $CH_4$ or Ar, was purified by passing it through a dry-ice acetone cooled 5 Å molecular sieve trap. The OCS gas was added to the carrier gas through a stainless steel capillary (0.1 mm × 1 m). The total pressure of the gaseous mixture in the ion source was a few torr and the partial pressure of OCS was varied from 10 to 100 mTorr. The gas mixture was ionized with a pulsed 2 keV electron beam, and the ions produced were sampled through a slit made with razor blades. The width of the slit was 10 $\mu$m and the length 1 mm. Since the width of the slit was smaller than the mean free path at a few torr of the carrier gas, the ions were sampled through the slit by molecular flow, i.e., adiabatic cooling of the effusing gas during the ion sampling was negligible.

Thermochemical data ($\Delta G^o$, $\Delta H^o$, and $\Delta S^o$) were obtained by measuring the temperature dependence of the equilibrium constant $K$ using the van't Hoff equation, $-\ln K = \Delta G^o/RT = \Delta H^o/RT - \Delta S^o/R$.

Cluster geometries of $OCS^+(OCS)_n$, $S_2^+(OCS)_1$, $H^+OCS(OCS)_n$, and $C_2H_5^+(OCS)_n$ were determined with the B3LYP/6-311G(d) method [9]. For the first three clusters, B3LYP/6-311+G(d,p) calculations were also carried out. After full geometry optimizations, vibrational analyses were performed to determine whether the geometries were correctly optimized for stable species and to obtain zero-point vibrational energies (ZPE). Isomeric structures were carefully examined. The $n = 1$ bond energies were also assessed using G2(MP2) calculations [10]. All calculations were carried out with the aid of Gaussian 98 program [11] installed at the Compaq ES40 in the Information Processing Center (Nara University of Education, Nara, Japan).

## Results and Discussion

### *Primary Ion/Molecule Reactions in OCS*

Using methane as carrier gas, $C_2H_5^+$ and $H^+(OCS)$ were the major ions detected. The primary ions produced from $CH_4$ by electron ionization were $CH_3^+$ and $CH_4^+$ with comparable abundance. These ions react with $CH_4$ to give $C_2H_5^+$ and $CH_5^+$, respectively. The proton affinity value of OCS (150.4 kcal/mol) is between those of $C_2H_4$ (162.8 kcal/mol) and $CH_4$ (130.0 kcal/mol) [12]. Thus, $CH_5^+$ reacts rapidly with OCS to form $H^+(OCS)$ according to reaction (1).

$$CH_5^+ + OCS + H^+(OCS) + CH_4 \quad (1)$$

The proton transfer reaction, $C_2H_5^+ + OCS \rightarrow H^+(OCS) + C_2H_4$, is endothermic, and the clustering reaction (eq 2) is the major process in the reaction of $C_2H_5^+$ with OCS.

$$C_2H_5^+(OCS)_{n-1} + OCS = C_2H_5^+(OCS)_n \quad (2)$$

Similarly, the $H^+(OCS)$ formed in the same experiments was observed to cluster with OCS as illustrated in reaction (eq 3).

$$H^+(OCS)(OCS)_{n-1} + OCS = H^+(OCS)(OCS)_n \quad (3)$$

The equilibrium constants for reactions (eq 2) and (eq 3) were measured to a temperature just above that of the OCS gas condensation point.

When Ar was used as carrier gas, $S^+$, $OCS^+$, and $S_2^+$ were major ions observed and $S_3^+$ was a minor ion. The following ion/molecule reactions are proposed in the presence of Ar.

$$Ar^+ + OCS = OCS^+ + Ar \quad (4\text{-}1)$$

$$Ar^+ + OCS = S^+ + CO + Ar \quad (4\text{-}2)$$

$$S^+ + OCS = S_2^+ + CO \quad (5)$$

$$OCS^+ + OCS = S_2^+ + 2CO \quad (6)$$

$$S_2^+ + OCS = S_3^+ + CO \quad (7)$$

The rate constants for reactions (eq 5), (eq 6), and [(eq 7) at 300 K have been reported as $5.4 \times 10^{-10}$], $3.2 \times 10^{-10}$, and $5.8 \times 10^{-12}$ $cm^3$/molecule·s, respectively [13].

The overall reaction (eq 4) proceeded with collision rate, as shown by the rapid decay of $Ar^+$ after the electron pulse. Rapid formation of $OCS^+$ and of $S_2^+$ was observed during the electron pulse. Furthermore, strong signals of $OCS^+(OCS)_n$ ions and $S_2^+(OCS)_n$ were recorded following the electron pulse, and equilibria for clustering reactions (eq 8) and (eq 9) were determined.

$$OCS^+(OCS)_{n-1} + OCS = OCS^+(OCS)_n \quad (8)$$

$$S_2^+ + OCS = S_2^+(OCS) \quad (9)$$

These observations indicate that the conversions of $OCS^+$ to $S_2^+$ by reaction (eq 6) and the conversion of $S_2^+$ to $S_3^+$ by reaction (eq 7) were slow under the present experimental conditions. The slow decay of $OCS^+$ is

inconsistent with the reported rate constant of $3.2 \times 10^{-10}$ cm$^3$/molecule·s for reaction (6), which predicts a reactive lifetime of $OCS^+$ of $\sim 1$ $\mu$s under the experimental conditions used [13]. This also implies that the $S_2^+$ ion is formed primarily by reaction (eq 4-2) [14], followed by reaction (eq 5), and not by reaction (eq 4-1) followed by reaction (eq 6), as would be expected based on the published rate constants. A weak $S_3^+$ signal was observed during the electron pulse. However, the relative intensity of this ion did not increase after the electron pulse. It could, therefore, be concluded that the rate constant of $5.8 \times 10^{-12}$ cm$^3$/molecule·s reported for reactions (eq 7) [13] is also overestimated.

Figure 1 shows the net atomic charges in the OCS molecule and the shape of the highest occupied molecular orbital (HOMO) (RB3LYP/6-311G*). It is seen that the HOMO has a large spatial extension on the sulfur atom, which facilitates electron-transfer (ET) toward cation species, such as $OCS^+$, $S_2^+$, $H^+OCS$, and $C_2H_5^+$. However, the sulfur atom is positively charged (+0.049e), which is unfavorable for the Coulombic interaction with a cation. Thus, if the ET interaction is weak, it can be expected that the negatively charged oxygen atom of OCS, and not the sulfur atom, would interact with a cation. Our study examines this bifunctionality of OCS toward cationic sites.

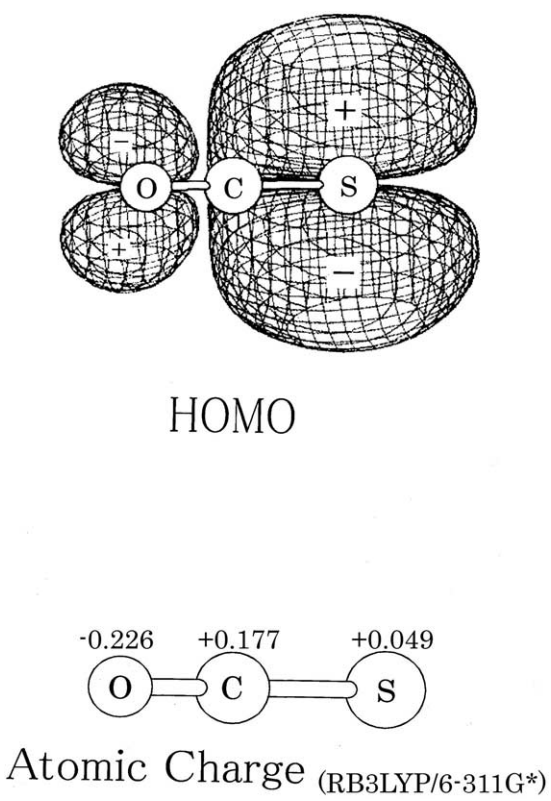


**Figure 1.** Orbital shape of the highest occupied molecular orbital (HOMO) and the net Mulliken atomic charge (the positive value, cationic) obtained at the level of RB3LYP/6-311G*.

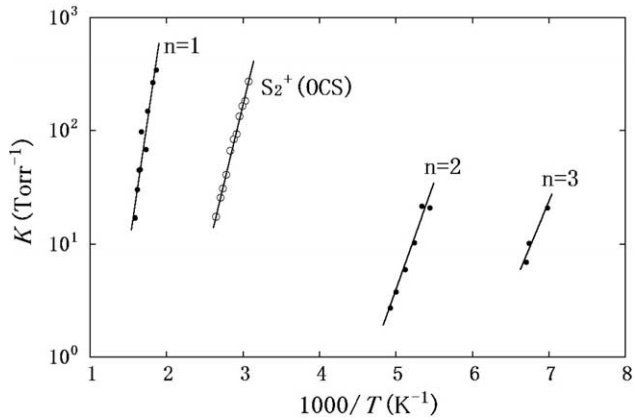


**Figure 2.** van't Hoff plots for clustering reactions for (filled circle): $OCS^+(OCS)_{n-1} + OCS = OCS^+(OCS)_n$ and (open circle): $S_2^+ + OCS = S_2^+(OCS)$.

## *Clustering Reactions of $OCS^+$ and $S_2^+$ with OCS*

Figure 2 depicts the van't Hoff plots for clustering reactions (eq 8) with $n = 1$–3. The thermochemical data obtained from the plots are summarized in Table 1.

A large gap is seen between the $n = 1$ and 2 in van't Hoff plots. The presence of such gap suggests that the positive charge in the complex $(OCS)_2^+$ is delocalized by electron-transfer, OCS → $OCS^+$, while the second ($n = 2$) OCS ligand interacts weakly with the $(OCS)_2^+$ complex. The formation of a *two-center three-electron* bond between the two sulfur atoms in $(OCS)_2^+$ with $C_2$ symmetry has been predicted by McKee [5] who calculated the bond energy for $[OCS \cdots SCO]^+$ as 19.9 kcal/mol. This theoretically derived value is smaller than our experimentally obtained value of 23.9 ± 2.0 kcal/mol. The present G2(MP2) value is 22.97 kcal/mol. Ono et al. [4] predicted the bond energy of $OCS^+(OCS)$ to be 17.2 ± 1 kcal/mol in their molecular beam photoionization study of OCS and $(OCS)_2$. Their reported value is much smaller than the value obtained here. The underestimated value in the Ono et al. study may be due to unfavorable Franck-Condon factors near the ionization thresholds, which would make it difficult to determine actual values of adiabatic ionization energies.

The OCS molecule is isovalent with $CO_2$ and $CS_2$, therefore, it is of interest to compare the bond energies of the dimer cations, $M_2^+$, of these molecules. For M = $CO_2$, OCS, and $CS_2$, the bond energies are 15.6 ± 1.0, [15] 23.9 ± 2.0 (measured in this study), and 24.9 ± 1.5 [16] kcal/mol, respectively. The ionization energies are 13.77 eV for $CO_2$, 11.17 eV for OCS, and 10.07 eV for $CS_2$. The stronger bonds in $(OCS)_2^+$ and $(CS_2)_2^+$ than that in $(CO_2)_2^+$ is thus explained by the formation of S ··· S bonds, with extensive electron-transfer (ET), in $(OCS)_2^+$ and $(CS_2)_2^+$ complexes. The *two-center three-electron* bond is likely to be formed by intermolecular orbital interactions. Scheme **1a** shows that ET contributes to the formation of the S ··· S bond. Configurations such as HOMO of OCS and SOMO of $OCS^+$ both have large orbital lobes on the sulfur atom. The (HOMO → SOMO)

**Table 1.** Experimental and theoretical data ($-\Delta H^0_{n-1,n}$ and $-\Delta S^0_{n-1,n}$) for clustering reactions, $A^+(OCS)_{n-1}$ + OCS = $A^+(OCS)_n$ for $A^+ = OCS^+$ and $H^+(OCS)$. $\Delta H^0_{n-1,n}$ and $\Delta S^0_{n-1,n}$ are in kcal/mol and cal/mol · K (standard state, 1 atm), respectively. $\Delta E_{n-1,n}$ (in kcal/mol) is the bonding energy calculated by B3LYP/6-311G* electronic and zero point vibrational energy (without parenthesis). Data in parentheses are by B3LYP/6-311+G(d,p), and those in square brackets are by G2(MP2). $\Delta E_{n-1,n}(A)$ and $\Delta E_{n-1,n}(B)$ are the computed bond energies of $OCSH^+(OCS)_n$ and $SCOH^+(OCS)_n$, respectively

| | $OCS^+(OCS)_n$ | | | $H^+(OCS)(OCS)_n$ | | | |
|---|---|---|---|---|---|---|---|
| n | $-\Delta H^0_{n-1,n}$ | $-\Delta E_{n-1,n}$ | $-\Delta S^0_{n-1,n}$ | $-\Delta H^0_{n-1,n}$ | $-\Delta E_{n-1,n}(A)$ | $-\Delta E_{n-1,n}(B)$ | $-\Delta S^0_{n-1,n}$ |
| 1 | 23.9 ± 2.0 | 27.45 | 19 ± 4 | 13.5 ± 1.0 | 11.83 | 19.16 | 21 ± 3 |
| | 17.2 ± 1[a] | (27.40) | | | (12.51) | (21.71) | |
| | | [22.97] | | | [11.29] | [18.51] | |
| 2 | 7.8 ± 0.4 | 7.89 | 23 ± 3 | 5.7 ± 0.3 | 6.89 | 4.94 | 19 ± 3 |
| | 1.6[a] | (7.92) | | | (6.93) | (4.02) | |
| 3 | 6.3 ± 1.0 | 4.62 | 25 ± 5 | 4.3 ± 0.5 | 6.20 | 4.51 | 13 ± 3 |
| | | (4.52) | | | (6.30) | (4.00) | |
| 4 | | 4.07 | | | 4.53 | 3.12 | |
| | | (4.08) | | | (4.66) | (3.16) | |
| 5 | | 3.73 | | | 4.23 | | |
| | | (3.66) | | | (4.17) | | |

[a]Reference [4].

ET, i.e., the electron delocalization, produces (S ··· S) semi-covalent bond. The (SOMO → LUMO) back ET in Scheme 1a also contributes to the bond formation. The bond is almost free from Coulombic repulsion, because the sulfur atom in OCS is nearly neutral (+0.049e in Figure 1). In contrast, the oxygen atom in $CO_2$ has more anionic character, and the O = C = O···O = C = $O^+$ geometry is improbable. Indeed, $(CO_2)_2^+$ is known to have the O = C = O···$CO_2^+$ coordination, in which the LUMO (not SOMO) of $CO_2^+$ is the electron acceptor. The explanation for the proposed twisted structure of $(OCS)_2^+$ ion is offered below. Assuming that the S···S one-site interaction through ET were the sole factor determining the geometry, a $C_{2h}$-symmetry trans geometry would be obtained. Such exchange interaction is depicted in Scheme 1b. In the typical configuration, the

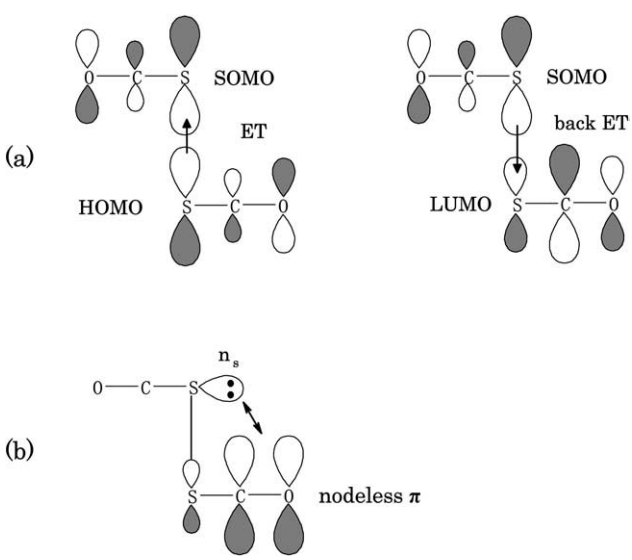


**Scheme 1.** Two orbital interactions leading to the $C_2$-symmetry geometry of $(OCS)_2^+$ ion.

trans planar geometry is subject to repulsion between the two doubly occupied orbitals, $n_S$ and the nodeless $\pi$. However, the repulsion would be eliminated in a twisted structure of $C_2$- symmetry.

Figure 3 depicts the geometries of $OCS^+(OCS)_n$ for $n$ = 1, 3, and 5 calculated with the B3LYP/6-311G(d) method. The geometries for $n$ = 2 and 4 were also obtained but are not presented for brevity. Our study found that the $n$ = 1 geometry had $C_2$ symmetry and that the cationic charge was delocalized in the two OCS moieties through a *two-center three-electron* bond, as discussed above. This is in agreement with the report by McKee [5]. The $n$ = 2 geometry was determined to be of Cs symmetry (figure not shown) with O = C = S···$(SCO)^+$··· S = C = O coordination. The character of a *two-center three-electron* bond is largely lost. Transition to a mainly electrostatic interaction of the cation with two neutral OCS molecules explains the large fall-off in the bond energies, 23.9 ± 2.0 → 7.8 ± 0.4 kcal/mol, (see Table 1). There are three geometric isomers for $n$ = 3. In $n$ = 3(a), the oxygen atom O(10) of the third OCS ligand is linked with S(2), S(4), and C(1). This triple coordination makes the $n$ = 3(a) cluster the most stable one. The $n$ > 2 clusters are controlled by electrostatic attractions. Sterically, the $n$ = 5 cluster is a saturation shell.

The computed bonding energies ($-\Delta E_{n-1,n}$) of the $OCS^+(OCS)_n$ cluster are shown in the left column of Table 1. The B3LYP $-\Delta E_{0,1}$ value of 27.45 (27.40 at zero point energy) kcal/mol, is somewhat larger than the experimental one, 23.9 ± 2.0 kcal/mol and the G2(MP2) energy (22.97 kcal/mol). However, the B3LYP $-\Delta E_{1,2}$ value of 7.89 (7.92 at zero point energy) kcal/mol, is in good agreement with the present experimental one of 7.8 ± 0.4 kcal/mol. The literature value of 1.6 kcal/mol, [4] is likely to be an underestimate.

The van't Hoff plot for clustering reaction (9) is shown in Figure 2. The $-\Delta H^o$ and $-\Delta S^o$ values were determined to be 12.9 ± 1 kcal/mol and 15 ± 2 cal/mol·K, respec-

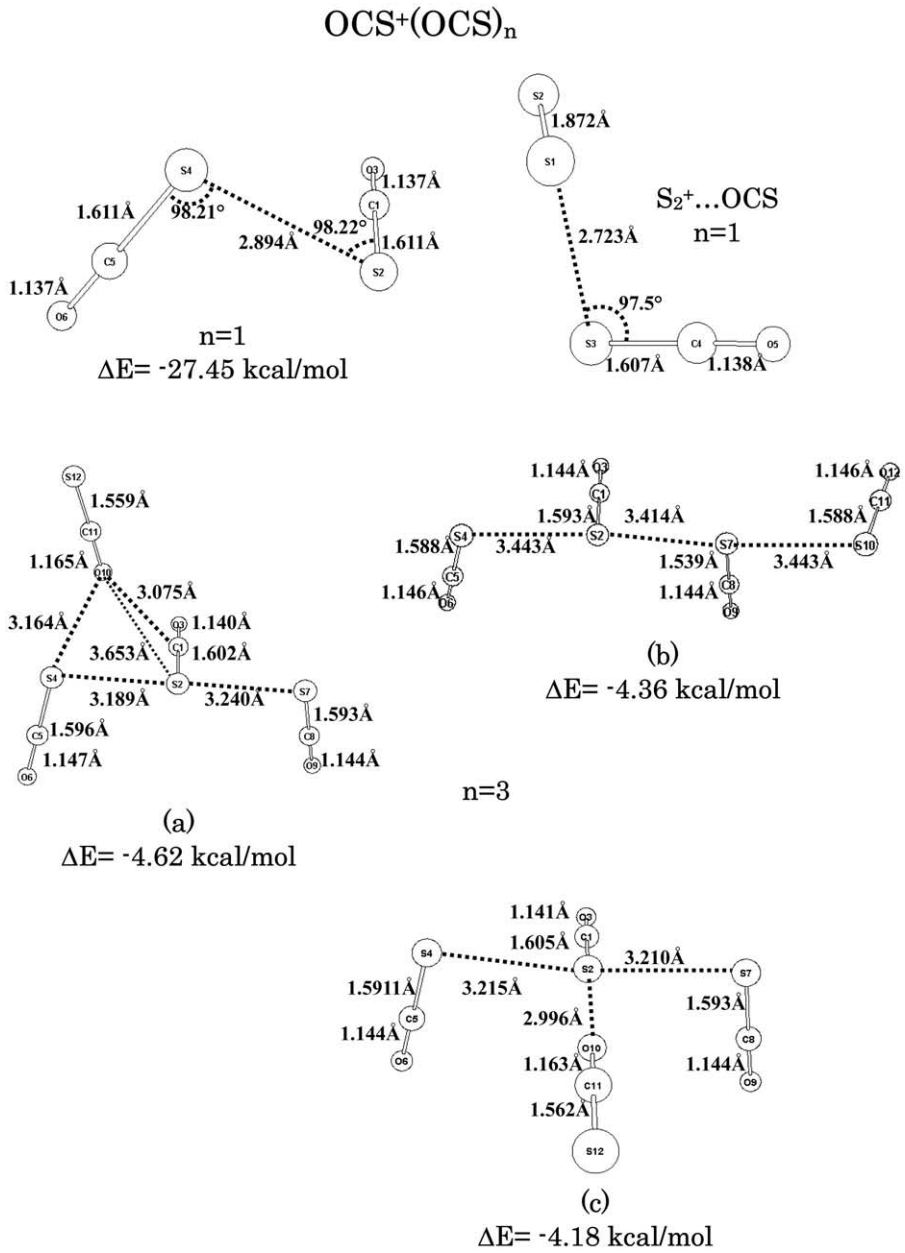


**Figure 3.** The geometries of $OCS^+(OCS)_n$ ($n$ = 1, 3, and 5) and $S_2^+(OCS)_1$ optimized by UB3LYP/6-311G(d). For $OCS^+(OCS)_3$, the stability order is (**a**) > (**b**) > (**c**). ΔE is the calculated interaction energy.

tively. The calculated bond energies are 15.49 [B3LYP/6-311G(d)], 14.88[B3LYP/6-311+G(d)], and 12.34[G2(MP2)] kcal/mol, respectively. In our previous work [16], the thermochemical stabilities and structures of $S_2^+(CS_2)_n$ were investigated. The $-\Delta H^o_{0,1}$ and $-\Delta S^o_{0,1}$ values for reaction (eq 10) were determined as 30.9 ± 1.5 kcal/mol and 25 ± 3 cal/mol·K, respectively.

$$S_2^+(CS_2)_{n-1} + CS_2 = S_2^+(CS_2)_n \quad (10)$$

It should be noted that the bond energy of $S_2^+(OCS)$ (12.9 ± 1 kcal/mol) is much smaller than that of the isovalent $S_2^+(CS_2)$ complex. In the latter complex, a linear but twisted shape, S–$S^+$···S–C–S with the formation of semi-covalent bond was predicted [16]. The weaker bond energy for $S_2^+(OCS)$ means that the (OCS → $S_2^+$) ET is much smaller than that for $S_2^+(CS_2)$. The HOMO energy of OCS is −169.43 kcal/mol (−0.27 a.u.;1 a.u. = 627.51 kcal/mol), (RHF/STO-3G*), and that of SCS is −138.05 kcal/mol (−0.22 a.u.), which suggests that OCS has a larger ionization potential (IP) than SCS. In fact, the B3LYP/6-311G* calculated IP values for OCS are IP(OCS) = 257.7 kcal/mol (11.18 eV) and for SCS IP(SCS) = 232.8 kcal/mol (10.10 eV), respectively. These theoretical values are in excellent agreement with quoted above experimental values of

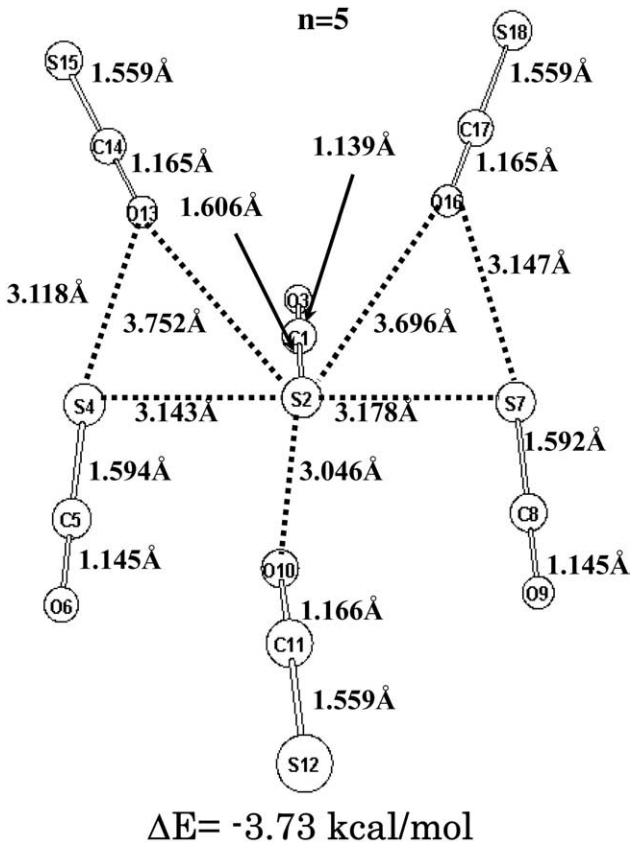


**Figure 3.** Continued

11.17 eV (OCS) and 10.07 eV (SCS). The inferior ET ability of OCS compared with that of SCS explains the lower bond energy value measured for the $S_2^+\cdots$OCS complex than bond energy value of $S_2^+\cdots$SCS complex.

The equilibrium constants for reaction $S_3^+$ + OCS = $S_3^+$(OCS) could not be measured due to weak signal intensities.

## *Clustering Reaction of $H^+$(OCS) with OCS*

The experimentally determined equilibrium constants for the formation of $H^+(OCS)(OCS)_n$, as specified in reaction (eq 3), are displayed as van't Hoff plots in Figure 4 and corresponding thermochemical data are listed in Table 1. As in the case of reaction (eq 8) (see Figure 2), there is a large gap in the van't Hoff plots between $n$ = 1 and 2. The existence of such gap suggests that a relatively strong semi-covalent bond is formed in the complex $H^+$(OCS)(OCS), while the interaction in the larger cluster ions $H^+(OCS)(OCS)_n$ with $n \geq 2$ is mainly electrostatic, and therefore, weaker.

Our previous study [17] revealed that the bond energies of proton held symmetric dimers $H^+(B)_2$ gradually decrease with an increase of the proton affinities of the bases, B. A larger electron dispersal in $H^+$–B due to a higher proton affinity correlates with an elevation of the $\sigma^*$(B–H) energy level and poor electron-accepting strength and will lead to weaker B–$H^+$–B bonding. The

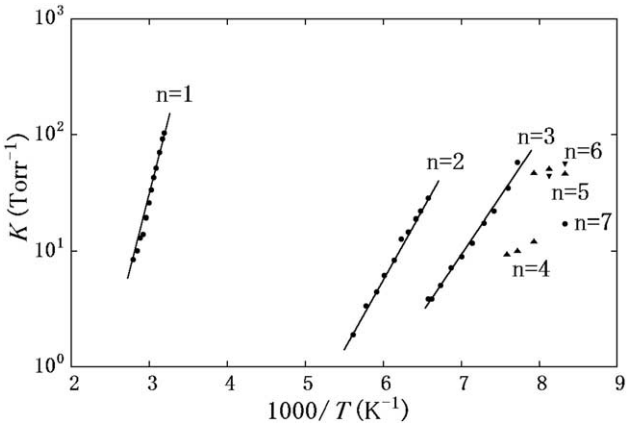


**Figure 4.** van't Hoff plots for clustering reactions $H^+(OCS)(OCS)_{n-1}$ + OCS = $H^+(OCS)(OCS)_n$.

bond energies of $H^+(B)_2$ for B = $CO_2$, COS, and $CS_2$ are measured to be 8.0 [18], 3.5 ± 1.0 (present study), and 9.0 ± 1.5 [19] kcal/mol, respectively. This is the reverse order of proton affinities for $CO_2$ (129.3 kcal/mol), COS (150.4 kcal/mol), and $CS_2$ (163.1 kcal/mol) [9]. Thus, the trend reported in our earlier investigation [17] was confirmed in the present work.

The equilibrium between $H^+$(OCS) and $H^+$(OCS)(OCS) was recorded in the temperature range of 360~300 K. The larger cluster ions, $H^+(OCS)(OCS)_n$ with $n \geq 2$, were observed only at temperatures below ~180 K (see Figure 4). The relative ion intensities become time-independent about 500 μs after the electron pulse and equilibrium constants were calculated using such intensities. It was confirmed that the equilibrium constants for reaction (eq 3) with $n$ = 1–3 were independent of the partial pressure of OCS in the range of 10–100 mTorr. The behavior of the cluster ion intensities as equilibrium was approached was highly unusual. This is illustrated in Figure 5, which demonstrates the time profiles of the normalized intensities for $H^+(OCS)(OCS)_n$ with $n$ = 0–3 after the electron pulse at 161.5 K (1000/$T$ = 6.19). The $H^+(OCS)(OCS)_3$ intensity shows an initial steep increase followed by a rapid decrease toward a time-independent value. The

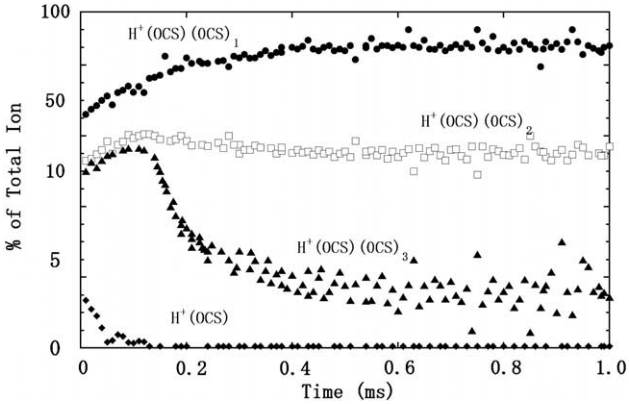


**Figure 5.** Temporal profiles of ions $H^+(OCS)(OCS)_n$ with $n$ = 0–3 observed in 2.47 torr $CH_4$ and 42 mTorr OCS at 161.5 K.

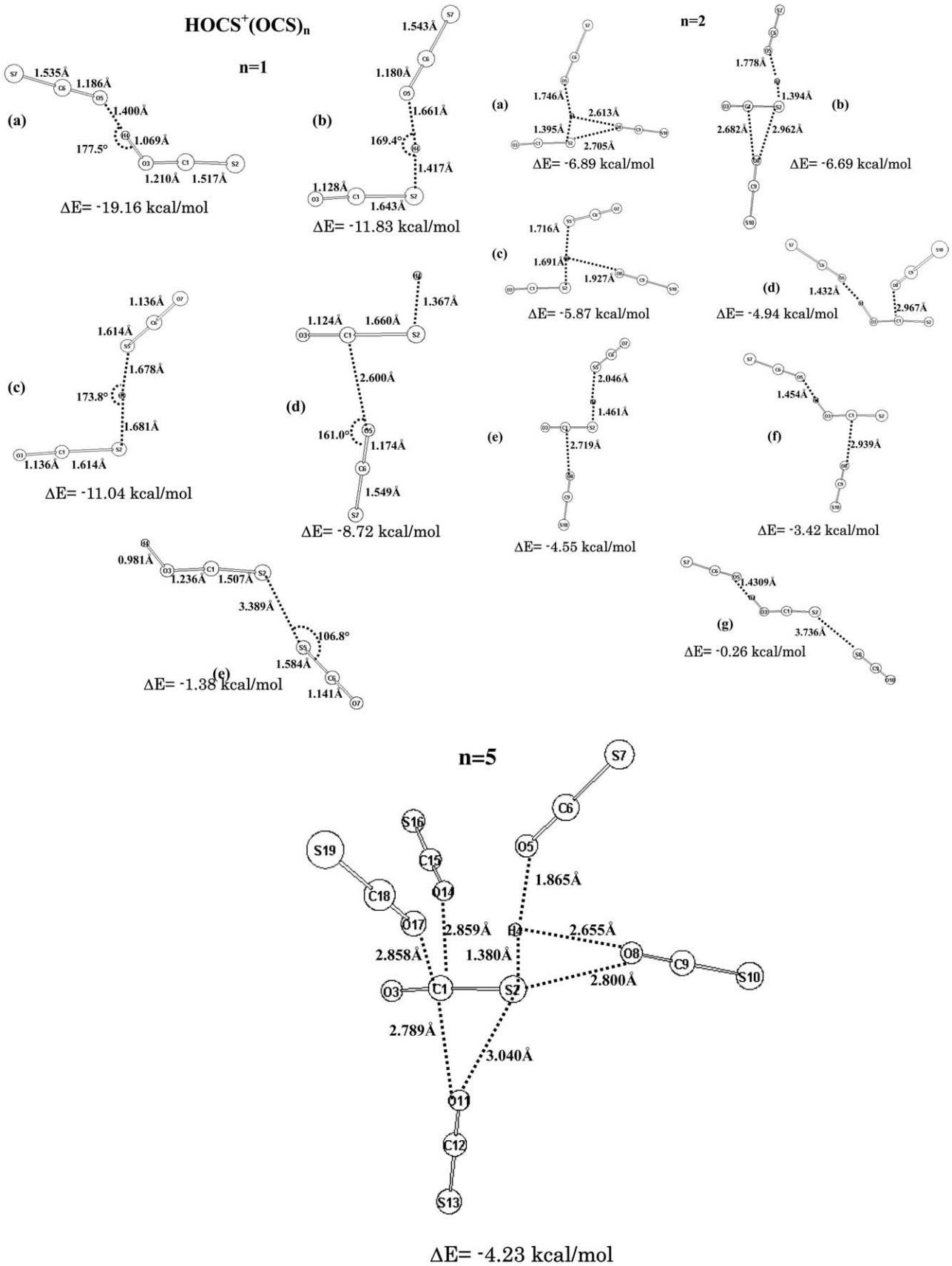


**Figure 6.** Geometries of $H^+(OCS)(OCS)_n$, $n$ = 1, 2, and 5 determined at the level of B3LYP/6-311G*.

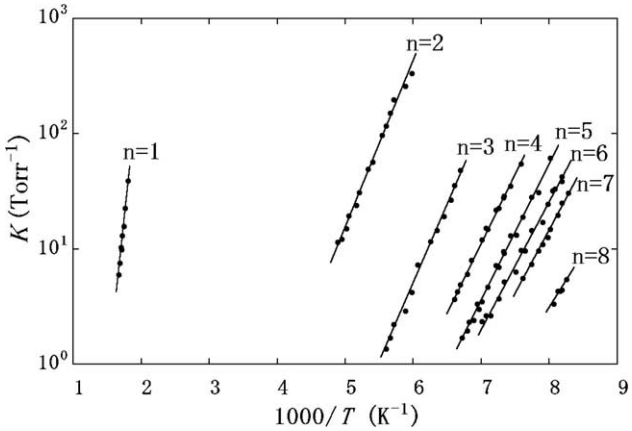


**Figure 7.** van't Hoff plots for the clustering reaction, $C_2H_5^+(OCS)_{n-1}$ + OCS = $C_2H_5^+(OCS)_n$. Those for $n$ = 5 are somewhat scattered, which is ascribed to coexistence of two structural isomers in text explanations.

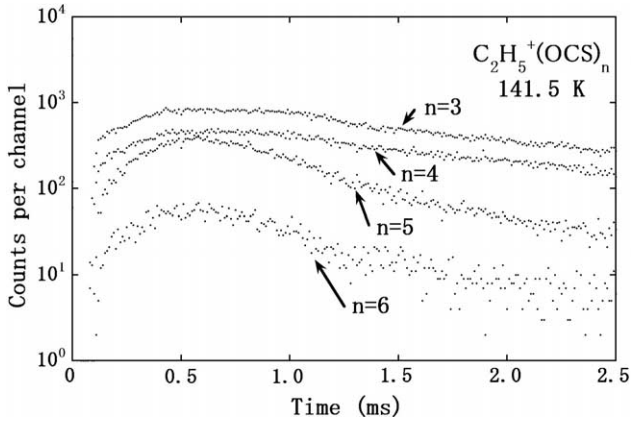


**Figure 8.** Temporal profiles of $C_2H_5^+(OCS)_n$ with $n$ = 3–6 observed in 2.18 torr $CH_4$ and 39 mTorr OCS. Ion source temperature = 141.5 K, energy of incident electron = 2 keV, electron pulse width = 700 $\mu$s. At 2.6 ms, a short positive pulse (25 V) is applied to annihilate all ions produced in the ion source. The integration time for the ions $C_2H_5^+(OCS)_n$ with $n$ = 3–6 are 60, 60, 60, and 120 s, respectively.

same pattern, although less pronounced, applies to $H^+(OCS)(OCS)_2$ cluster. In contrast, the intensity of the $H^+(OCS)(OCS)$ cluster shows a steady increase and becomes time-independent after ~600 $\mu$s. The typically observed behavior is that the intensities of the largest clusters increase monotonically because larger clusters are formed from smaller ones. The unusual behavior (see Figure 5) suggests that, in our case, the larger cluster ions are gradually converted to smaller ones. A possible explanation is that the $H^+(OCS)(OCS)_n$, $n$ = 1 and 2, cluster ions are composed of more than one isomer; that the initially formed isomers are thermochemically less stable, and that these are gradually converted to more stable isomers. The proposed scenario is supported by the calculations, as discussed below.

With decrease of temperature below ~130 K, cluster ions $H^+(OCS)(OCS)_n$ with $n \geq 4$ were formed. However, equilibria for reaction (eq 3) with $n \geq 4$ could not be determined. The equilibrium constants with $n \geq 4$ shown in Figure 4 were arbitrarily calculated from the ion intensities about 2 ms after the electron pulse. The erratic van't Hoff plots with $n \geq 4$ in Figure 4 indicate that the cluster populations contain several isomeric ions.

There are several possible isomeric structures for $H^+(OCS)(OCS)_n$. Since the proton affinity of $CS_2$ (163.1 kcal/mol) is much larger than that of $CO_2$ (129.3 kcal/mol) [9], the S-atom protonated OCS (i.e., $OCSH^+$) is expected to be the most stable form of protonated OCS. Although the dipole moment of OCS ($\mu$ = 0.71 D) [20] is not large, the O atom of OCS is highly negatively charged (see Figure 1). Therefore, also O-atom protonated OCS (i.e., $SCOH^+$) might be formed by reaction (eq 1). RB3LYP/6-311G* calculations indicate that $H^+$–OCS is only 5.44 kcal/mol ($\Delta E$, the difference of total energies and ZPEs) less stable than OCS–$H^+$. Diverse geometries of possible isomers of $H^+(OCS)(OCS)_n$, $n$ = 1, and $n$ = 2, based on theoretical calculations (B3LYP/6-311G*), are presented in Figure 6. Suffixes (a), (b), (c), . . . show the stability ranking with (a) being more stable than (b), etc. It was found that while O–C–S–$H^+$···O–C–S [$n$ = 1(b)] is based on the most stable protonated species (O–C–S–$H^+$), it is not the most stable isomer. Instead, the most stable dimer is S–C–O–$H^+$···O–C–S [$n$ = 1(a)], which is built on the less stable protonated specie (S–C–O–$H^+$). In contrast, the most stable $n$ = 2(a) complex is that of SCO···O–C–S–$H^+$···O–C–S, which

**Table 2.** Experimental thermochemical data ($-\Delta H^0_{n-1,n}$ and $-\Delta S_{n-1,n}$) and the computed bonding energy ($\Delta E_{n-1,n}$) for clustering reaction, $C_2H_5^+(OCS)_{n-1,n}$ + OCS = $C_2H_5^+(OCS)_n$. $\Delta H^0_{n-1,n}$ and $\Delta S^0_{n-1,n}$ are in kcal/mol and cal/mol · K (standard state, 1 atm), respectively. $\Delta E_{n-1,n}$ values (in kcal/mol) are theoretical energies calculated by RB3LYP/6-311G* electronic and zero-point vibrational energies. $\Delta E_{n-1,n}(A)$ and $\Delta E_{n-1,n}(B)$ are for classical and nonclassical $C_2H_5^+$ moieties, respectively

| | $C_2H_5^+(OCS)_n$ | | | |
|---|---|---|---|---|
| n | $-\Delta H^0_{n-1,n}$ | $-\Delta E_{n-1,n}$ (A) | $-\Delta E_{n-1,n}$ (B) | $-\Delta S^0_{n-1}$ |
| 1 | 24.9 ± 2.0 | **21.39** | 9.46 | 25 ± 3 |
| 2 | 7.1 ± 0.3 | **6.12** | 5.94 | 17 ± 3 |
| 3 | 6.5 ± 0.3 | **5.50** | 5.53 | |
| 4 | 5.8 ± 0.3 | **5.01** | 3.92 | 22 ± 3 |
| 5 | ~5.5 | 3.19 | **4.00** | ~23 |
| 6 | 5.3 ± 0.3 | 2.92 | **3.38** | 23 ± 3 |
| 7 | 5.2 ± 0.2 | 2.49 | **2.57** | 24 ± 3 |
| 8 | 4.7 ± 0.4 | | | 22 ± 5 |

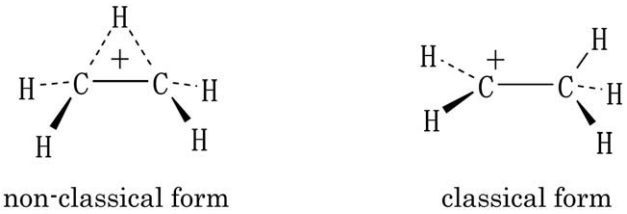


**Scheme 2.** Two geometric isomers of ethyl cation.

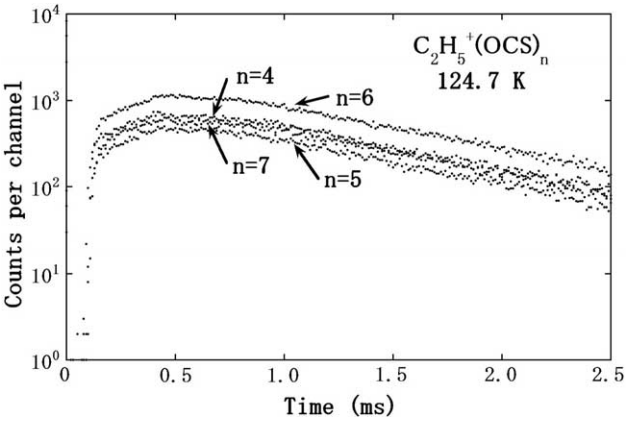


**Figure 9.** Temporal profiles of $C_2H_5^+(OCS)_n$ with $n$ = 4–7 observed in 2.03 torr $CH_4$ and 36 mTorr OCS. Ion source temperature = 124.7 K, energy of incident electron = 2 keV, electron pulse width = 700 $\mu$s. At 2.6 ms, a short positive pulse (25 V) is applied to annihilate all ions produced in the ion source. The integration time for the ions $C_2H_5^+(OCS)_n$ with $n$ = 4–7 are 90, 30, 60, and 60 s, respectively.

contains the stable O–C–S–$H^+$ cation (Figure 6, $n$ = 2). Similarly, for the larger clusters with $n > 2$, the most stable isomer is the one that contains S-protonated OCS. The $n$ = 5 cluster has a saturation shell (Figure 6, $n$ = 5).

While the electronic charge in SCO–$H^+$–OCS is dispersed because of the formation of a strong hydrogen bond in the complex, the charge in $OCSH^+\cdots OCS$ is more localized in the $OCSH^+$ core ion. In fact, loss of electron charge from the neutral OCS in $n$ = 1(a) is 0.16e, while it is 0.11e in $n$ = 1(b). Due to charge localization in $OCSH^+$, the electrostatic interactions in OCS–$H^+\cdots(OCS)_n$ are expected to be stronger than in SCO–$H^+$–SCO$\cdots(OCS)_{n-1}$. The isomerization of initially formed $OCSH^+\cdots(OCS)_n$ clusters to the thermodynamically more stable $n$ = 1(a) structures, would explain the successive conversion to smaller cluster ions, $H^+(OCS)(OCS)_3 \rightarrow H^+(OCS)(OCS)_2 \rightarrow H^+(OCS)(OCS)_1$ in Figure 5. When equilibrium is reached, after about 600 $\mu$s in Figure 5, the cluster ions should be composed mainly of the most stable structures shown in Figure 6. The isomerization reaction may proceed via an intracluster proton transfer reaction in the $H^+(OCS)_2$ moiety, i.e., OCS–$H^+\cdots$OCS $\rightarrow$ OCS$\cdots H^+$–OCS. The isomerization reactions become progressively slower at lower temperature, probably due to the presence of an energy barrier for the intramolecular proton transfer reaction.

In Table 1, two calculated energies, $-\Delta E_{n-1,n}$(A) and $-\Delta E_{n-1,n}$(B), are shown. For $n \geq 2$, binding energies of $-\Delta E_{n-1,n}$(A) are larger than those of $-\Delta E_{n-1,n}$(B). At $n$ = 1 $\rightarrow$ 2, there is a switch of cluster series, B $\rightarrow$ A.

## *Clustering Reaction of $C_2H_5^+$ with OCS*

The experimentally measured equilibrium constants for reaction (eq 2) are displayed as van't Hoff plots in Figure 7, and the derived enthalpy and entropy changes ($\Delta H^o_{n-1,n}$, and $\Delta S^o_{n-1,n}$) are summarized in Table 2.

Due to weak bonding, the larger $C_2H_5^+(OCS)_n$, $n \geq 2$, cluster ions were only observed below ~204 K. Measurements of equilibrium constants for reaction (eq 2) were straightforward for the smaller clusters with $n$ = 1–4, as these equilibria were established quickly. However, the approach to equilibrium was much slower for the larger clusters with $n > 4$. This is illustrated in Figure 8, which shows temporal profiles of the cluster ions $C_2H_5^+(OCS)_n$ with $n$ = 3–5 measured at 141.5 K. It is seen that the equilibrium between the $n$ = 3 and $n$ = 4 clusters is established already during the electron pulse, as shown by the fact that the ratio of the abundances maintains a constant value. The equilibrium between the $n$ = 5 and $n$ = 6 clusters is also quickly established. However, the equilibrium between the $n$ = 4 and $n$ = 5 clusters is approached very slowly and the ratio of the abundances of these clusters is still changing after 2.5 ms. Therefore, equilibrium constants for this reaction were calculated from intensities measured at 2–3 ms after the electron pulse. The scatter in the van't Hoff plots with $n$ = 5 in Figure 7 indicates that the equilibrium was not established even after 2–3 ms. The fast establishment of equilibria between $C_2H_5^+(OCS)_n$-clusters with $n \leq 4$, on the one hand, and between clusters with $n \geq 5$, on the other, while the equilibrium between the two groups is approached very slowly, suggest that the core ions $C_2H_5^+$ have different structures in the two groups. This issue will be considered next.

In our previous work [21], the thermochemical stabilities and structures of the gas-phase cluster ions $C_2H_5^+(Sol)_n$ (Sol = $CO_2$ and $N_2O$) were studied. For the free, nonsolvated $C_2H_5^+$ ion, it was concluded that only the nonclassical structure exists and the classical one is absent (Scheme 2). In the solvated clusters, on the other hand, $C_2H_5^+$ was found to preferentially adopt the classical form.

There is a large gap between the $n$ = 1 and 2 lines in Figure 7, and the $-\Delta H^o_{n-1,n}$ values show a corresponding large drop from $n$ = 1 (24.9 ± 2.0 kcal/mol) to $n$ = 2 (7.1 ± 0.3 kcal/mol). The strong binding in the $C_2H_5^+(OCS)_1$ cluster constitutes evidence that the $C_2H_5^+$ ion forms a semi-covalent bond with the OCS ligand. This implies that the $C_2H_5^+$ ion has the classical structure. The weak interactions in the clusters with $n \geq 2$ indicate that the bonding of OCS in these clusters is mainly electrostatic in nature.

In Figure 8, it was seen that the abundances of the larger cluster ions with $n$ = 5 and 6 decreased faster than those with $n \leq 4$. Thus, the larger cluster ions ($n \geq 5$) are gradually converted to smaller ones ($n \leq 4$). This is analogous to the behavior observed for $H^+(OSC)(OCS)_n$ clusters in Figure 5. We conjecture that the classical structure is the most stable form of the $C_2H_5^+$ core ion in the smaller clusters, $C_2H_5^+(OCS)_n$, $n \leq 4$, whereas the nonclassical structure is the most stable form in the larger ($n \geq 5$) clusters. Additionally, it is

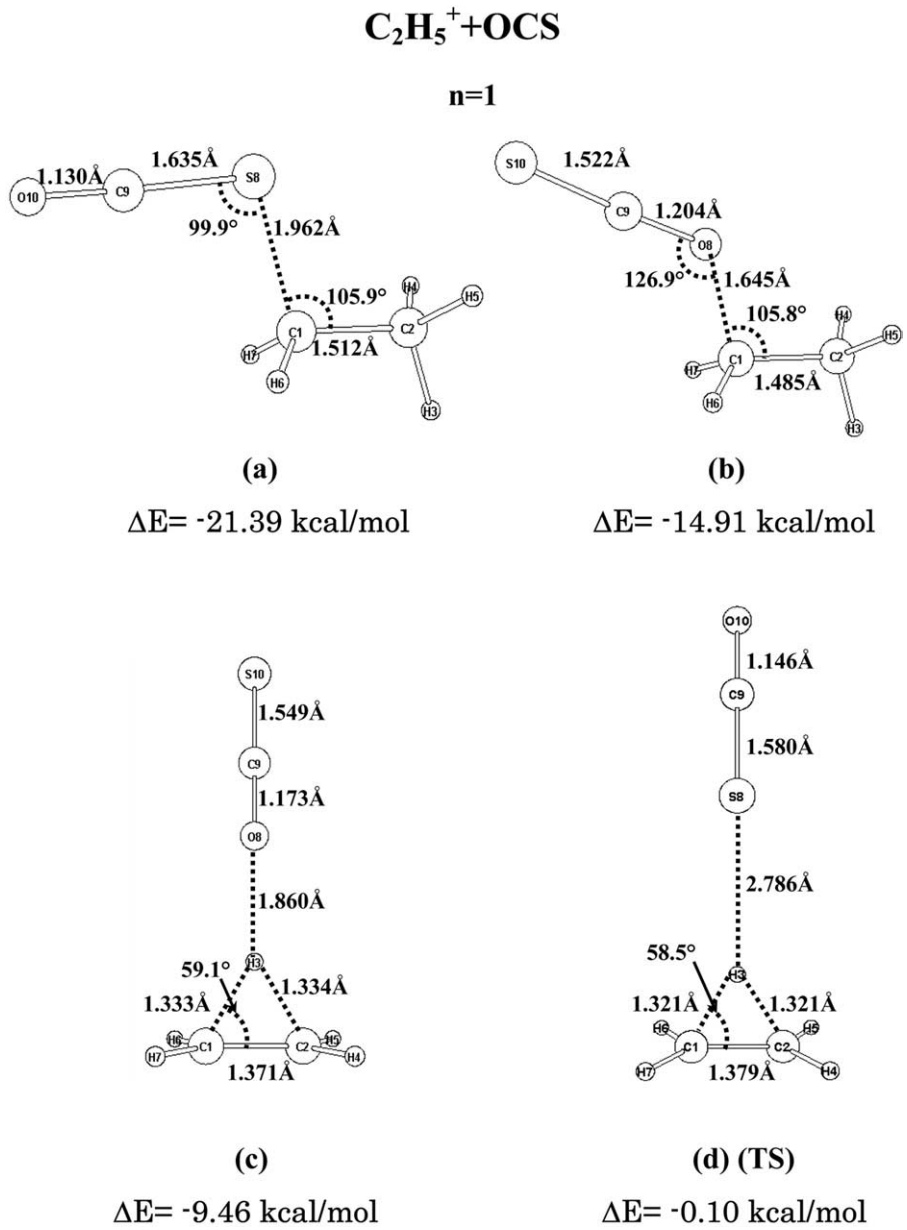


**Figure 10.** Geometries of $C_2H_5^+(OCS)_1$ optimized by RB3LYP/6-311G*. Distances are in Å. $n$ = 1(**d**) (TS) means that the isomer **1**(**d**) is not at an energy minimum but at a saddle point. Stability of the four geometric isomers is in the order, **1**(**a**) > **1**(**b**) > **1**(**c**) > **1**(**d**).

assumed that all clusters, when formed at temperatures of 150 K or lower, initially retain the nonclassical form of free $C_2H_5^+$. However, the $C_2H_5^+$ core ion gradually isomerizes from the nonclassical to the classical structure, and this is accompanied by the formation of a strong bond with one OCS ligand. With the nonclassical structure, the positive charge is mainly localized in $C_2H_5^+$, resulting in relatively strong electrostatic interactions with OCS ligands. However, when $C_2H_5^+$ isomerizes to the classical $C_2H_5^+$ structure and forms a semi-covalent bond with OCS, the positive charge will be dispersed in $C_2H_5^+(OCS)_1$. This charge delocalization results in weaker electrostatic interactions with additional OCS ligands and changes the relative stabilities of different sized clusters. This would explain the faster decay of $C_2H_5^+(OCS)_n$ ($n$ = 5 and 6) than those with $n$ = 3 and 4 in Figure 8.

With decreasing temperature, the difference in the decay rates of $C_2H_5^+(OCS)_n$ with $n \leq 4$ and $\geq 5$ became smaller. This may be due to a slowdown of the isomerization reaction of $C_2H_5^+$ from the nonclassical to the classical structure at lower temperature. Figure 9 shows the temporal profiles of $C_2H_5^+(OCS)_n$ with $n$ = 4–7 measured at 124.7 K (1000/T ≈ 8). The equilibria for all cluster ions were established already during the electron pulse. It seems likely that the isomerization reaction is practically forbidden at this low-temperature. There is an increased gap between the van't Hoff plots for $n$ = 5 and 6 in Figure

7, both of which were measured at 1000/T ≥ 8. This suggests that the shell structure for the less stable cluster ions was completed with $n = 7$.

The conclusions above are supported by the calculations as shown next. Figure 10 shows four geometric isomers of $C_2H_5^+(OCS)_1$. Figure 10a and b show complexes with the classical $C_2H_5^+$-containing isomer, and Figure 10c and d show complexes with the nonclassical $C_2H_5^+$ isomer. The isomers containing the classical structure were found to be more stable. Furthermore, as expected from the shape of the HOMO (Figure 1), the S-bridged structure, **1**(a), is more stable than the O-bridged structure, **1**(b). For the nonclassical $C_2H_5^+$ ion, the order is reversed and, as expected from the atomic charges, **1**(c) is more stable than **1**(d). Indeed, **1**(d) is not even a bound state, but represents a transition-state (TS) with two imaginary frequencies. Contact of the soft atom (sulfur) with the bridge-head hydrogen of $C_2H_5^+$ immediately leads to **1**(a). Thus, the energy barrier raised above comes from rotation of the O=C=S bond on the $C_2H_5^+$ moiety [i.e., isomerization **1**(c) → **1**(a)].

Figure 11 shows calculated geometries of $C_2H_5^+(OCS)_7$. The $n = 7$(a) geometry is composed of the

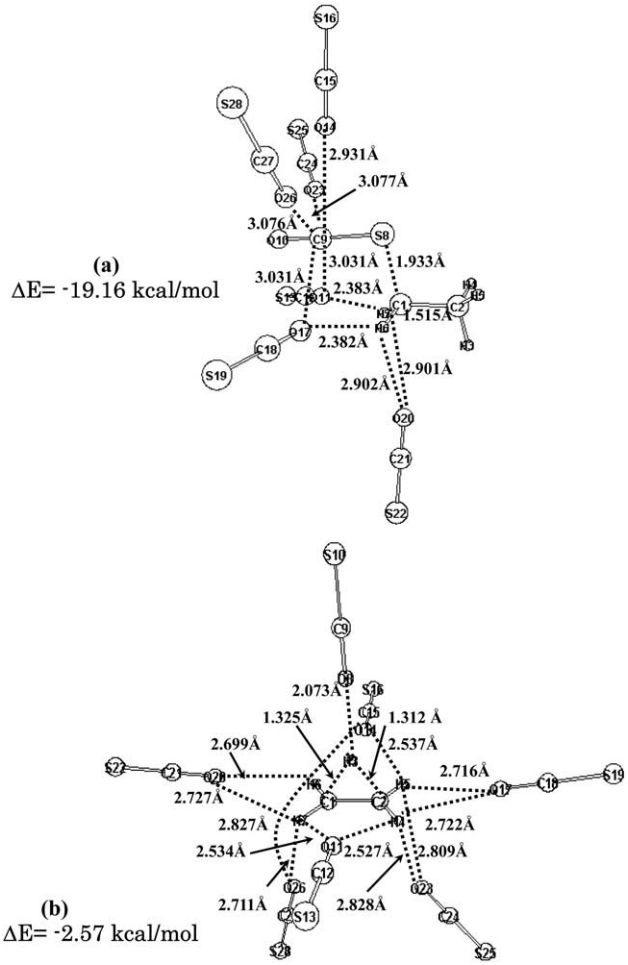


**Figure 11.** Geometries of two $C_2H_5^+(OCS)_7$ isomers obtained from those of $n$ = **1**(**a**) and $n$ = **1**(**c**), respectively.

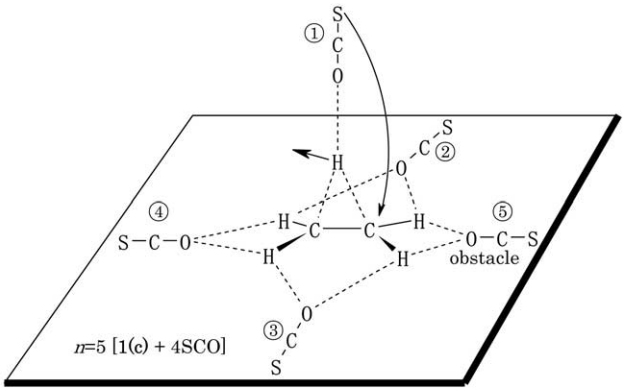


**Scheme 3.** To convert the nonclassical $C_2H_5^+$ to the classical one, the fifth (numeral 5 in circle) ligand must be excluded.

classical $C_2H_5^+$ core ion and seven OCS molecules, while the $n = 7$(b) geometry contains the nonclassical $C_2H_5^+$ ion. Both 7(a) and 7(b) are of the saturated form. Although 7(a) is definitely more stable than 7(b), the 7(b) structure predominates at low temperatures. The serial numbers, (numeral 1 in circle), (numeral 2 in circle), (numeral 5 in circle), in Scheme 3, show that the less sterically hindered OCS ligands interact with $C_2H_5^+$ preferably in the $n = 7$(b), i.e., $n = 1$(c) + 6SCO isomer. In this geometry, the fifth (numeral 5 in circle) OCS ligand is an obstacle for isomerization to the 1(a)-based series.

In other words, the $n \leq 4$ clusters may take the more stable 1a-based geometries.

When the clusters are formed at low temperatures, the charge-controlled **1**(c) series is generated primarily. As the temperature is raised, the ligand (OCS) fluctuation becomes active. For $n \leq 4$, rotation of the on-top OCS molecule leads to the isomerization to the **1**(a) series clusters.

Table 2 displays the calculated binding energies ($-\Delta E_{n-1,n}$) for two series of clusters (A and B). Bold ones through the "bypass" are in good agreement with the present experimental data. The bypass point, $n = 4 \rightarrow 5$, is consistent with the discussions based on the experimental data, although the calculated energies of $n \geq 6$ are somewhat underestimated relative to the observed ones.

## Conclusions

The bifunctional OCS molecule has been studied in clustering reactions with four cations, $OCS^+$, $S_2^+$, $H^+SCO$, and $C_2H_5^+$. It has been of mechanistic interest to examine the relation of the bifunctionality to the clustering pattern. In $OCS^+(OCS)_n$ and $S_2^+(OCS)_1$ clusters, S···S bonds are primarily formed with 23.9 ± 2 and 12.9 ± 1 kcal/mol ($n = 1$) bond energies, respectively. $OCS^+(OCS)_n$ ($n \geq 2$) has small bond energies owing to the charge delocalization in $OCS^+(OCS)_1$. The bifunctionality of OCS has afforded geometric isomers of $H^+(OCS)(OCS)_n$ and $C_2H_5^+(OCS)_n$ clusters. Whereas

OCS–$H^+$ is more stable than $H^+$–OCS, OCS–$H^+$···OCS is less stable than SCO···$H^+$–OCS. This causes anomalous temporal profiles in HPMS experiments (Figure 5). The bridged nonclassical form of the ethyl cation is preserved in $n$ = 5–8 of $C_2H_5^+(OCS)_n$. For $n < 5$, the classical form $C_2H_5^+$ is attained through isomerization. The $C_2H_5^+(OCS)_n$ species underwent the two-series clusters via the bypass without the serious contamination of van't Hoff plots. The experimental binding energies are in fair agreement with calculated ones. Coexistence of two geometric isomers may be recognized experimentally, when the pattern of covalent bonds of central cations is changed (e.g., $H^+OCS \rightarrow OCSH^+$ and $H^+C_2H_4 \rightarrow H_3C–CH_2^+$.

OCS is stable in the troposphere (300 ~ 220 K) and is supplied to the stratosphere (220 ~ 270 K) where it contributes to the formation of stratospheric aerosol. So far, limited studies have been performed on ion/molecule reactions taking place in the stratosphere. In this work, it is shown that the bifunctionality of OCS may play important roles for the formation of various sulfur compounds in the stratosphere and interstellar medium.

## References


1. Thornton, D. C.; Bandy, A. R.; Blomquist, B. W.; Anderson, B. E. Impact of anthropogenic and biogenic sources and sinks on carbonyl sulfide in the North Pacific troposphere. *J. Geophys. Res. Atmos.* **1996,** *101,* 1873.
2. Palumbo, M. E.; Geballe. T. R.; Tielens, A. G. G. M. Solid carbonyl sulfide (OCS) in dense molecular clouds. *Astrophys. J.* **1997,** *479,* 839.
3. Xu, X.; Bingemer, H. G.; Schmidt, U. The flux of carbonyl sulfide and carbon disulfide between the atmosphere and a spruce forest. *Atmos. Chem. Phys. Discussion* **2002,** *2,* 181.
4. Ono, Y.; Osuch, E. A.; Ng, C. Y. Molecular beam photoionization study of OCS, $(OCS)_2$, $(OCS)_3$, and OCS-$CS_2$. *J. Chem. Phys.* **1981,** *74,* 1645.
5. McKee, M. L. Ab initio study of the $(OCS)_2^+$ complex. *Chem. Phys. Lett.* **1991,** *179,* 559.
6. Lugez, C. L.; Thompson, W. E.; Jacox, M. E. The infrared spectra of $OCS^+$ and OCS- trapped in solid neon. *J. Chem. Phys.* **2001,** *115,* 166.
7. Kebarle, P. Pulsed electron high pressure mass spectrometer. In *Techniques for the Study of Ion-Molecule Reactions*; Farrar, J. M.; Saunders, W. H., Eds.; Wiley: New York, 1988, p. 221.
8. Hiraoka, K. A determination of the stabilities of $H_3^+(H_2)_n$ with n = 1–9 from measurements of the gas-phase ion equilibria $H_3^+$ $(H_2)_n$–1 + H2 = $H_3^+$(H2)n. *J. Chem. Phys.* **1987,** *87,* 4048.
9. Becke, A. D. Density-functional thermochemistry. III. The role of exact exchange. *J. Chem. Phys.* **1993,** *98,* 5648.
10. Curtiss, L. A.; Raghavachari, K.; Pople, J. A. Gaussian-2 theory using reduced Møller-Plesset orders. *J. Chem. Phys.* **1993,** *98,* 1293.
11. Frisch, M. J.; Trucks, G. W.; Schlegel, H. B.; Scuseria, G. E.; Robb, M. A.; Cheeseman, J. R.; Zakrzewski, V. G.; Montgomery, J. A.; Stratmann, R. E.; Burant, J. C.; Dapprich, S.; Millam, J. M.; Daniels, A. D.; Kudin, K. N.; Strain, M. C.; Farkas, O.; Tomasi, J.; Barone, V.; Cossi, M.; Cammi, R.; Mennucci, B.; Pomelli, C.; Adamo, C.; Clifford, S.; Ochterski, J.; Petersson, G. A.; Ayala, P. Y.; Cui, Q.; Morokuma, K.; Malick, D. K.; Rabuck, A. D.; Raghavachari, K.; Foresman, J. B.; Cioslowski, J.; Ortiz, J. V.; Stefanov, B. B.; Liu, G.; Liashenko, A.; Piskorz, P.; Komaromi, I.; Gomperts, R.; Martin, R. L.; Fox, D. J.; Keith, T.; Al-Laham, M. A.; Peng, C. Y.; Nanayakkara, A.; Gonzalez, C.; Challacombe, M.; Gill, P. M. W.; Johnson, B.; Chen, W.; Wong, M. W.; Andres, J. L.; Head-Gordon, M.; Replogle, E. S.; Pople, J. A. *Gaussian 98, Revision A. 7*; Gaussian, Inc., Pittsburgh PA, **1998**.
12. Hunter, E. P. L.; Lias, S. Evaluated gas phase basicities and proton affinities of molecules: an update. *J. Phys. Chem. Ref. Data* **1998,** *27,* 413.
13. Dzidic, I.; Good, A.; Kebarle, P. Ion-molecule reactions in carbonyl sulfide-hydrocarbon mixtures. *Can. J. Chem.* **1970,** *48,* 664.
14. Dotan, I.; Lindinger, W. Energy dependences of the reactions of $Ar^+$ with $H_2$, $N_2$, CO, $O_2$, $CO_2$, $N_2O$, and COS. *J. Chem. Phys.* **1982,** *76,* 4972.
15. Hiraoka, K.; Nakajima, G.; Shoda, T. Determination of the stabilities of $CO_2^+(CO_2)_n$ and $O_2^+(CO_2)_n$ clusters with n = 1–6. *Chem. Phys. Lett.* **1988,** *146,* 535.
16. Hiraoka, K.; Fujimaki, S.; Aruga, K.; Yamabe, S. Frontier-controlled structures of the gas-phase A ± $(CS_2)_n$ clusters, A± = $S_2^+$, $CS_2^+$, $S_2^-$, and $CS_2^-$. *J. Phys. Chem.* **1994,** *98,* 1802.
17. Hiraoka, K.; Takimoto, H.; Yamabe, S. Gas-phase stabilities of symmetric proton-held dimer cations. *J. Phys. Chem.* **1986,** *90,* 5910.
18. Hiraoka, K.; Shoda, T.; Morise, K. Yamabe, S. Kawai, E.; Hirao, K. Stability and structure of cluster ions in the gas phase: Carbon dioxide with $Cl^-$, $H_3O^+$, $HCO_2^+$, and $HCO^+$. *J. Chem. Phys.* **1986,** *84,* 2091.
19. Hiraoka, K.; Fujimaki, S.; Aruga, K.; Yamabe, S. Proton-held dimer and trimer of carbon disulfide. *Chem. Phys. Lett.* **1993,** *202,* 167.
20. Gierke, T. D.; Tigelaar, H. L.; Flygare, W. H. Calculation of molecular electric dipole and quadrupole moments. *J. Am. Chem. Soc.* **1972,** *94,* 330.
21. Hiraoka, K.; Shoda, T.; Kudaka, I.; Fujimaki, S.; Mizuse, S.; Yamabe, S. H.; Wasada-Tsutsui, Y. Gas-phase study of the clustering reactions of $C_2H_5^+$, $s^-C_3H_7^+$, and $t^-C_4H_9^+$ with $CO_2$ and $N_2O$: isomeric structure of $C_2H_5^+$, $C_2H_5^+(CO_2)_n$, and $C_2H_5^+(N_2O)_n$. *J. Phys. Chem. A* **2003,** *107,* 775.